



# Live imaging reveals a biphasic mode of dissemination of *Borrelia burgdorferi* within ticks

Star M. Dunham-Ems,<sup>1</sup> Melissa J. Caimano,<sup>1</sup> Utpal Pal,<sup>2,3</sup> Charles W. Wolgemuth,<sup>4,5</sup> Christian H. Eggers,<sup>6</sup> Anamaria Balic,<sup>7</sup> and Justin D. Radolf<sup>1,8</sup>

<sup>1</sup>Department of Medicine, University of Connecticut Health Center, Farmington, Connecticut, USA. <sup>2</sup>Department of Veterinary Medicine, University of Maryland, College Park, Maryland, USA. <sup>3</sup>Virginia-Maryland Regional College of Veterinary Medicine, College Park, Maryland, USA.

<sup>4</sup>Department of Cell Biology and <sup>5</sup>Center for Cell Analysis and Modeling, University of Connecticut Health Center, Farmington, Connecticut, USA.

<sup>6</sup>Department of Biomedical Sciences, Quinnipiac University, Hamden, Connecticut, USA. <sup>7</sup>Department of Craniofacial Sciences and

<sup>8</sup>Department of Genetics and Developmental Biology, University of Connecticut Health Center, Farmington, Connecticut, USA.

Lyme disease is caused by transmission of the spirochete *Borrelia burgdorferi* from ticks to humans. Although much is known about *B. burgdorferi* replication, the routes and mechanisms by which it disseminates within the tick remain unclear. To better understand this process, we imaged live, infectious *B. burgdorferi* expressing a stably integrated, constitutively expressed GFP reporter. Using isolated tick midguts and salivary glands, we observed *B. burgdorferi* progress through the feeding tick via what we believe to be a novel, biphasic mode of dissemination. In the first phase, replicating spirochetes, positioned at varying depths throughout the midgut at the onset of feeding, formed networks of nonmotile organisms that advanced toward the basolateral surface of the epithelium while adhering to differentiating, hypertrophying, and detaching epithelial cells. In the second phase of dissemination, the nonmotile spirochetes transitioned into motile organisms that penetrated the basement membrane and entered the hemocoel, then migrated to and entered the salivary glands. We designated the first phase of dissemination “adherence-mediated migration” and provided evidence that it involves the inhibition of spirochete motility by one or more diffusible factors elaborated by the feeding tick midgut. Our studies, which we believe are the first to relate the transmission dynamics of spirochetes to the complex morphological and developmental changes that the midgut and salivary glands undergo during engorgement, challenge the conventional viewpoint that dissemination of Lyme disease-causing spirochetes within ticks is exclusively motility driven.

## Introduction

Almost half of the world’s population is at risk for acquiring a potentially life-threatening vector-borne disease, such as malaria, dengue, Chagas disease, and plague (1). Conventional approaches for decreasing the prevalence of these infections have focused primarily on reducing or eliminating vector populations (2). A number of factors, most notably the emergence of pesticide-resistant vectors, highlight the need for novel control strategies (3). The rational design of preventive measures requires a detailed understanding of pathogen-vector interactions throughout the transmission process. Microorganisms transmitted by hematophagous arthropods have evolved specialized developmental programs that enable them to capitalize on vulnerabilities created by the remodeling of vector tissues during the blood meal in order to gain access to their vertebrate hosts (4–6). Confocal microscopy of fluorescent microbes has provided investigators with a powerful methodology for visualizing the discrete steps by which live organisms disseminate within the arthropod (7–9).

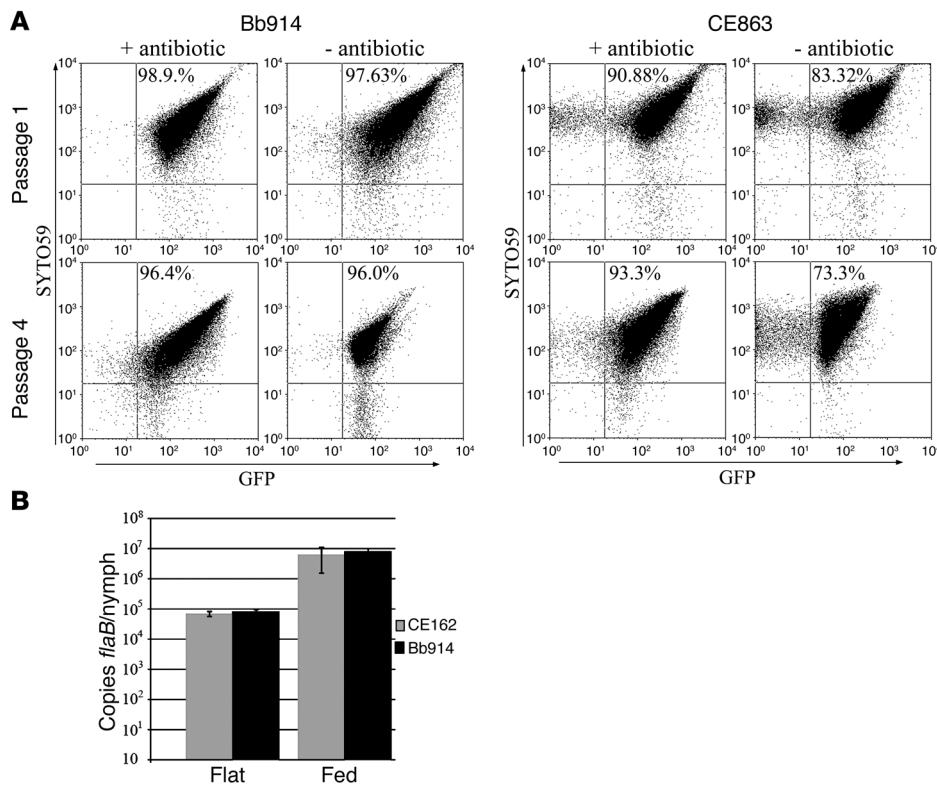
Lyme disease, caused by the spirochete *Borrelia burgdorferi*, is the most common arthropod-borne infection in the United States (10). If untreated, Lyme disease can lead to a wide array of complications typically involving the heart, joints, or nervous system

(11). *B. burgdorferi* cycles between 2 physiologically distinct environments, represented by the arthropod vector (*Ixodes* ticks) and mammalian host (11, 12). During larval acquisition, spirochetes colonize the midgut, which then remains infected through subsequent molts into the nymphal and adult stages. The nymphal stage is the most clinically relevant because it is usually responsible for the transmission of spirochetes to humans, an accidental host outside of the enzootic cycle (11, 12). Nymphal feeding induces the exponential expansion of spirochetes and migration of organisms out of the midgut into the hemocoel (13, 14), a process facilitated by the acquisition of plasminogen (15, 16). Once in the hemocoel, Lyme disease spirochetes must contend with the primary mediators of tick innate immunity, hemocytes and defensins, as they navigate toward the salivary glands (15, 17). Following attachment to the surface of the glands, spirochetes penetrate the surrounding basement membrane and are conveyed by the saliva into the dermis of the mammalian host (18–20).

While differential gene expression by *B. burgdorferi* and the kinetics of spirochete replication during the nymphal blood meal have been investigated extensively (12–14, 21–24), the routes and mechanisms that *Borrelia* utilize to disseminate within the tick have received considerably less attention. Here, we imaged live, infectious *B. burgdorferi* expressing a stably integrated, constitutively expressed GFP reporter in order to elucidate the interactions between spirochetes and *Ixodes scapularis* tissues during the nymphal blood meal. Our investigations revealed that *B. burgdorferi*

**Conflict of interest:** Justin D. Radolf has significant equity holdings in Johnson & Johnson, Pfizer, and General Electric and receives royalties from Biokit SA.

**Citation for this article:** *J. Clin. Invest.* 119:3652–3665 (2009). doi:10.1172/JCI39401.

**Figure 1**

Bb914 stably maintains a GFP reporter while retaining wild-type infectivity for ticks. **(A)** Flow cytometric comparison of Bb914 ( $P_{flaB}$ - $gfp$  inserted into cp26) and CE863 ( $P_{flaB}$ - $gfp$  in the shuttle vector pCE323) (34) grown to mid-logarithmic phase following temperature shift in the presence or absence of antibiotics. The percentages of GFP<sup>+</sup>/SYTO59<sup>+</sup> spirochetes are indicated in the upper-right-hand quadrant of each cytogram. Each flow cytogram is representative of 3 independent experiments. **(B)** Spirochete burdens of Bb914- and CE162-infected nymphs before and after feeding on naive C3H/HeJ mice. The infected nymphs used in these studies were generated by feeding naive larvae on syringe-inoculated C3H/HeJ mice as described in Methods. Data represent the means from 3 independent experiments; errors bars indicate SD.

progress through the feeding tick via a novel, biphasic mode of dissemination. In the first phase, spirochetes, positioned at varying depths throughout the midgut epithelium at the onset of feeding, replicate extensively, forming networks of nonmotile organisms that advance toward the basolateral surface of the epithelium while adhering to differentiating, hypertrophying, and detaching epithelial cells. This process, which we have designated “adherence-mediated migration,” involves the inhibition of spirochete motility by one or more diffusible factors elaborated by the feeding midgut. The second phase of dissemination is marked by the transition of nonmotile spirochetes into motile bacteria that then complete the penetration of the midgut, traverse the hemocoel, and migrate to and penetrate the salivary glands en route to the mammal. This motile, invasive phenotype continues throughout mammalian infection, ending when spirochetes colonize the midguts of feeding naive larvae to complete their enzootic cycle. Our studies, the first, to our knowledge, to relate the transmission dynamics of Lyme disease spirochetes to the complex morphological and developmental changes that *Ixodes* tick midguts and salivary glands undergo during engorgement, challenge the conventional viewpoint that spirochetal dissemination within ticks is exclusively motility driven.

## Results

*Bb914* stably maintains a GFP reporter while retaining wild-type infectivity for mice and ticks. Studies by us (25) and others (26) have demonstrated that borrelial shuttle vectors can be lost over time in the absence of selection during *in vivo* growth. We reasoned that insertion of a  $gfp$  expression cassette into cp26, a highly stable, endogenous borrelial plasmid (27, 28), would prevent loss of the fluorescent reporter during the extensive replication of spi-

rochetes that occurs following the nymphal blood meal (14, 29), thereby enhancing our ability to track organisms in locales where bacterial burdens are known to be low (e.g., hemolymph and salivary glands) (15, 18, 30, 31). To this end, Bb914 was generated by inserting  $gfp$  under the control of the constitutive  $flaB$  promoter ( $P_{flaB}$ - $gfp$ ) into the *bbb20-bbb21* intergenic region of cp26 in CE162, a virulent *B. burgdorferi* 297 clone (32) (Supplemental Figure 1; supplemental material available online with this article; doi:10.1172/JCI39401DS1). Bb914 and CE162 displayed essentially identical *in vitro* growth kinetics (data not shown) and protein expression profiles following temperature shift and cultivation within dialysis membrane chambers (DMCs) (Supplemental Figure 2). Of note, the levels of outer surface protein C (OspC) expressed by temperature-shifted and DMC-cultivated Bb914 and CE162 were highly similar (Supplemental Figure 2), indicating that insertion of the  $P_{flaB}$ - $gfp$  cassette did not alter transcription of *ospC* (*bbb19*), a gene essential for infectivity (26, 33). The fluorescent properties of Bb914 *in vitro* were compared with those of CE863, a CE162 transformant harboring  $P_{flaB}$ - $gfp$  on a cp32-derived shuttle vector (34), using flow cytometry. Virtually all Bb914 retained the cp26-borne  $gfp$  reporter in the absence of antibiotic, whereas CE863 cultured without selection contained a substantial nonfluorescent population that increased with repeated passaging (Figure 1A). Bb914 also was brighter than CE863, as indicated by a significantly greater mean fluorescence intensity value ( $324 \pm 47$  and  $228 \pm 24$ , respectively, for passage 1;  $P = 0.0227$ ).

Bb914 and CE162 possessed comparable infectivity ( $ID_{50}$  values of 116 and 224, respectively;  $P = 0.9462$ ) as measured by syringe inoculation of C3H/HeJ mice. Importantly, all Bb914 isolated from ear biopsies obtained 4 weeks after injection were GFP positive in the absence of antibiotic selection (data not shown). To assess the

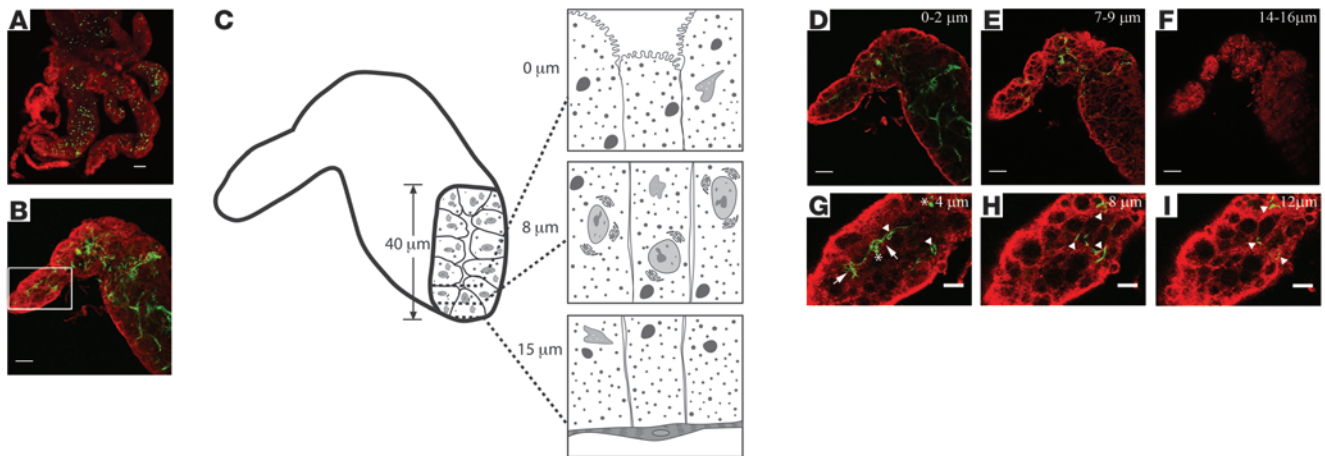


**Figure 2**

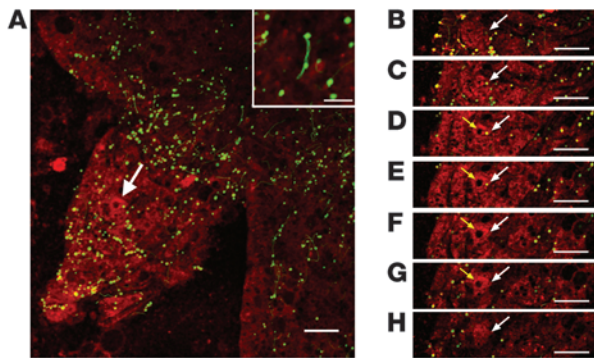
*B. burgdorferi* are distributed throughout the midguts of flat nymphs. (A) Low-power epifluorescence image of an isolated unfed midgut. (B) Composite confocal image showing the distribution of spirochetes through the full thickness (40 μm) of an unfed midgut. (C) Scheme used to acquire optical sections through an unfed Bb914-infected midgut and cartoon depiction of the cellular morphology at varying depths within the epithelium (modeled after ref. 46). (D–F) 3-μm composite images of optical sections acquired (D) at the luminal surface, (E) midway through the epithelium, and (F) at the basement membrane. (G–I) Digital enlargements of single, 1-μm optical sections of the boxed area in B acquired (G) at the luminal surface, (H) midway through the epithelium, and (I) at the most distal point where spirochetes were observed. Arrows, arrowheads, and asterisks indicate spirochete aggregates, intercellular spirochetes, and extracellular blebs, respectively; localization of spirochetes and blebs was determined by optical sectioning. Here and elsewhere, red staining denotes FM4-64; green staining denotes GFP. Scale bars: 50 μm (A); 25 μm (B, D–F); 10 μm (G–I).

ability of GFP-positive *Borrelia* to be acquired and maintained by ticks, naive *I. scapularis* larvae were allowed to feed on either BALB/c SCID or C3H/HeJ mice 2 weeks following intradermal syringe inoculation with a dose of  $1 \times 10^4$  Bb914. All Bb914-infected larvae examined at the time of repletion contained numerous fluorescent spirochetes, while quantitative PCR (qPCR) confirmed that Bb914 survived the larval molt and expanded during the nymphal blood meal as efficiently as its parent, CE162 (Figure 1B). Spirochete burdens were essentially identical in flat (i.e., unfed) and fed nymphs regardless of whether the starting larvae had fed on BALB/c SCID or C3H/HeJ mice infected with Bb914 (Supplemental Figure 3). Indirect immunofluorescence assay (IFA) studies demonstrated that the percentage of Bb914 expressing OspC at 72 hours after placement ( $44.7\% \pm 6.79\%$ ) was highly similar ( $P > 0.05$ ) to that previously observed for CE162 ( $49.43\% \pm 2.25\%$ ) (35) (Supplemental Figure 4), further establishing that the insertion in cp26 had no effect on OspC expression. Finally, we confirmed that *I. scapularis* nymphs infected with Bb914 could efficiently transmit spirochetes to naive C3H/HeJ mice when allowed to feed for 72 hours or longer; at 4 weeks after infection, 18/18 mice fed on by Bb914-infected nymphs were culture positive for GFP-expressing spirochetes.

*B. burgdorferi* are distributed throughout the midgut in flat nymphs. The intense autofluorescence of the *Ixodes* cuticle (36) necessitates the removal of midguts and salivary glands prior to examination by fluorescence microscopy. Previous immunofluorescence analyses of spirochetes within infected tick tissues have utilized nuclear stains (e.g., propidium iodide) to delineate midgut epithelial and salivary gland acinar cells (14, 19, 20, 33, 37). Given that *B. burgdorferi* are believed to be predominantly extracellular in ticks (38–40), we reasoned that visualization of cellular borders would enable us to localize spirochetes more precisely within midguts and salivary glands. For this purpose, we chose N-(3-triethylammoniumpropyl)-4-(p-diethylaminophenyl)-hexatrienyl pyridinium dibromide

(FM 4-64), a nontoxic lipophilic styryl dye that has been used to label the plasma membranes of a variety of eukaryotic cell types (41, 42). This dye also has been used to study the dissemination of malarial ookinetes within isolated midguts of *Anopheles* mosquitoes (8). In preliminary studies, FM4-64 clearly resolved epithelial cell boundaries within midgut diverticula that were gently nicked to allow ingress of the dye but was excluded from freshly isolated, intact midguts. The dye also readily stained freshly isolated salivary glands, providing extraordinary definition of acinar morphology (see below). Equally important, FM4-64 did not label *B. burgdorferi* and had no effect on spirochete viability or motility at a concentration more than 5 orders of magnitude greater than that used to label infected tick tissues (data not shown).

Consistent with the relatively high burdens detected by qPCR (Figure 1B), spirochetes within unfed nymphal midguts were easily visualized at low power as scattered green foci (Figure 2A) and, at higher magnification (Figure 2B), were found nearly throughout the full depth (~40 μm) of multiple diverticula. Organisms were most prevalent proximal to the stomach and diminished in density toward the distal ends of the diverticula (Figure 2, A and B). The distribution of spirochetes was analyzed by acquiring optical sections parallel to the long axis of a diverticulum through the full thickness of the midgut (see Figure 2C for image acquisition scheme). While the majority of spirochetes in unfed midguts were localized to the luminal surface of the epithelium, often forming small aggregates (Figure 2D), individual organisms frequently extended from the lumen into the intercellular spaces (Figure 2, E and G). Spirochetes, predominantly single organisms, also were readily apparent below the luminal surface, extending as far as 70% through the midgut epithelial layer (Figure 2, E, H, and I) but never reaching the basement membrane (Figure 2F). GFP-containing vesicles (i.e., blebs) were observed sporadically on and between epithelial cells (Figure 2G).

**Figure 3**

Spirochetes shed myriad blebs during early feeding (24 hours after placement). (A) Composite confocal image showing the distribution of spirochetes and numerous blebs through the full thickness of a midgut (45  $\mu\text{m}$ ); shown in the inset is a spirochete shedding blebs. Arrow indicates the cell in the consecutive confocal sections in B–H. (B–H) Localization of an intracellular bleb (arrow) present within A by consecutive 0.5- $\mu\text{m}$  confocal sections acquired through the full depth (3.5  $\mu\text{m}$ ) of an epithelial cell. N, nucleus. Scale bars: 25  $\mu\text{m}$ .

*Spirochetes progress through the nymphal midgut during feeding as epithelial cell-associated networks.* During the first 24 hours of attachment (the “preparatory phase”), when ticks establish a feeding site, little to no blood enters the midgut (43–46). At the 24-hour time point, we observed a slight thickening of the midgut (~45  $\mu\text{m}$ ), most likely due to an influx of interstitial fluid, without an obvious increase in epithelial cell size. Two changes related to the spirochetes were prominent. First, although the density and distribution of spirochetes appeared to be unchanged, numerous organisms were shedding blebs (Figure 3A). Second, myriad blebs were distributed throughout the midgut (Figure 3A). In contrast to the sporadic extracellular blebs observed in the unfed midgut (Figure 2G), the majority of blebs present during early feeding were determined to be intracellular based on consecutive optical sections and the presence of rims of FM4-64 (Figure 3, B–H).

At 48 hours after placement, we observed an obvious thickening of the midgut (~60  $\mu\text{m}$  at full thickness) due to an influx of blood as well as the differentiation and hypertrophy of epithelial cells. The composite image in Figure 4A demonstrates an increase in the density of spirochetes at 48 hours after placement compared with the unfed and 24-hour time points. In contrast to the 24-hour time point, we observed relatively few spirochetes shedding blebs and a marked reduction in both intracellular and extracellular GFP-positive vesicles. Spirochetes now were abundant within the lumen as single organisms and on the luminal surface as sizable aggregates extending intercellularly (Figure 4B). Particularly noteworthy was the increased number and size of spirochetal aggregates located entirely below the luminal surface (Figure 4C); in many cases, the leading edges of the aggregates extended to within 2  $\mu\text{m}$  of the basement membrane (data not shown), but, as with the previous time point, did not reach this structure (Figure 4D).

At 72 hours after placement, there was a marked distension of the midgut (>90  $\mu\text{m}$ ) due to the large volume of blood in the luminal space, now teeming with organisms (Figure 4, E and I). During this late stage of feeding, differentiating digestive cells hypertrophy, detach from the basement membrane, and are replaced by smaller undifferentiated cells that repeat the digestive cycle (43,

45, 46). Results from our confocal imaging of 72-hour-fed midguts (Figure 4, E–H and J–I) were in accord with the well-recognized asynchronous nature of this developmental sequence (43, 45, 46). In thicker areas of the midgut, where the epithelial cells were markedly hypertrophied (Figure 4, E–H), spirochetes reached near confluence on the luminal surface (Figure 4F), while dense aggregates extended from the lumen to form elaborate networks that essentially encased individual epithelial cells (Figure 4G). Identical networks of spirochetes were observed by confocal as well as epifluorescence microscopy regardless of whether the specimens were mounted in Vectashield, immersion oil, CMRL-1066 (CMRL), or Barbour-Stoenner-Kelley-II (BSK-II) medium (Supplemental Figure 5). In contrast to the 48-hour time point, organisms now were observed at the basolateral pole of the epithelial layer (Figure 4H); analysis of consecutive optical sections and orthogonal views revealed that some spirochetes at or near the basement membrane were wedged between epithelial cells in a “head-on” orientation (Figure 4H). In other regions of the midgut, the epithelial layer was substantially thinner (Figure 4, I–L), presumably because it consists mainly of undifferentiated cells (43, 45, 46). Although spirochetes were numerous in these areas, including at the basement membrane (Figure 4L), they did not reach the same level of confluence observed in the hypertrophied regions (Figure 4, compare E and I with the orthogonal views in H and L). Here, too, spirochetes in a head-on orientation could be identified between epithelial cells.

*Spirochetes advance around and between epithelial cells toward the basement membrane.* To further correlate the distribution of spirochetes with epithelial cell growth and differentiation during feeding, we examined silver-stained paraffin sections and FM4-64-labeled cryosections of midguts isolated at 48 and 72 hours after placement. At the 48-hour time point, hypertrophy of the epithelial cells was prominent, with some larger differentiated cells budding into the lumen (Figure 5, A and D). Spirochetes were distributed as individual organisms and as focal aggregates attached to the luminal surface and also wedged between epithelial cells, without any obvious preference for cell type. Consistent with the long axis confocal images of 48-hour-fed midguts (Figure 4, A–D), cryosectioning clearly demonstrated that organisms deeply penetrated the intercellular spaces but generally stopped short of the basement membrane (Figure 5, A and D). As noted above, by 72 hours after placement, the midgut epithelium either was markedly distended and sloughing cells into the lumen (Figure 5B) or consisted primarily of a thin layer of undifferentiated cells (Figure 5, C and E). In thicker areas of the midgut, spirochetes outlined many of the hypertrophied and detached epithelial cells in a manner reminiscent of the networks depicted by the long axis optical sections (compare Figure 4G and Figure 5B). In regions consisting predominantly of undifferentiated cells, the epithelial layer was markedly thinner and the spirochete densities were substantially lower (Figure 5, C and E). Cryosections of these areas highlighted the perpendicular orientation of spirochetes directly adjacent to the basement membrane (Figure 5F).

*Spirochetes within intact flat and fed midguts are nonmotile but respond differently when the midgut environment is breached.* *B. burgdorferi* is known for its vigorous motility in vitro (47, 48). During routine monitoring of intact 48-hour- and 72-hour-fed midguts by epifluorescence microscopy, as well as during the confocal analyses described above, we were surprised that the spirochetes did not appear to be motile. The lack of motility within the lumen and at varying depths

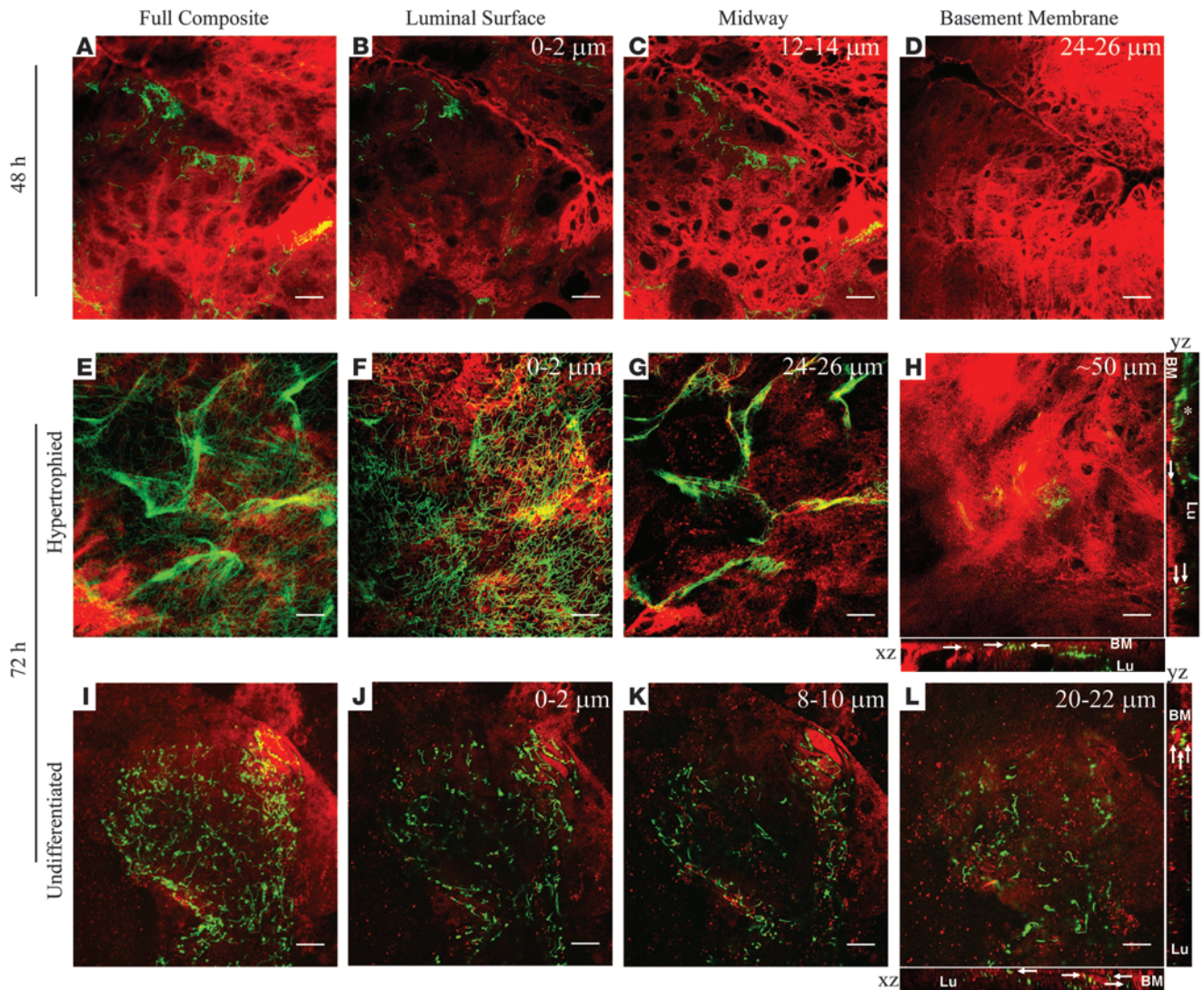


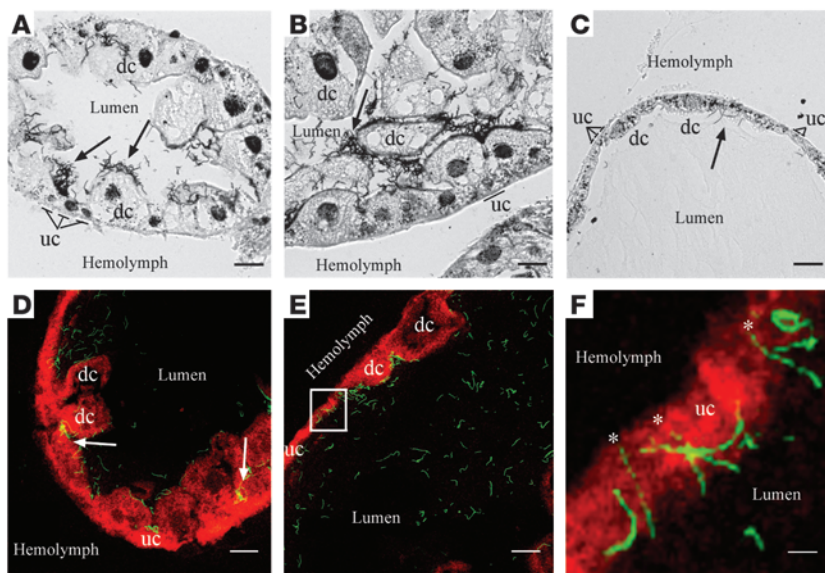
**Figure 4**

*B. burgdorferi* progress through the nymphal midgut during feeding in the form of epithelial cell-associated networks. Representative confocal micrographs of midguts isolated from Bb914-infected nymphs at (A–D) 48 and (E–L) 72 hours after placement; E–H and I–L, respectively, show hypertrophied and undifferentiated regions of 72-hour-fed midguts. Composite images in A, E, and I depict the full thickness of the respective epithelial layers. 3- $\mu$ m composite images show spirochetes (B, F, and J) at the luminal surface (C, G, and K) midway through the epithelium and (D, H, and L) at the basement membrane. Orthogonal views (y-z and x-z axes) for the 72-hour-fed midguts in H and L show that some spirochetes near the basement membrane (arrows) are in a head-on orientation. The positions of the lumen (Lu) and basement membrane (BM) in each orthogonal view are indicated. The asterisk in the y-z axis view of H denotes a spirochetal network. Scale bars: 25  $\mu$ m.

throughout the epithelial layer was confirmed by time-lapse confocal imaging of numerous intact (i.e., excluding FM4-64) midguts isolated at 48 and 72 hours after attachment (data not shown and Supplemental Video 1, respectively) and was observed regardless of the type of mounting medium used (data not shown). After the time-lapse imaging was completed, we assessed the viability of spirochetes within the imaged specimens by crushing the midguts in CMRL or BSK-II medium; the resulting suspensions contained numerous, highly motile organisms that were cultivatable in BSK-II and formed colonies on solid-phase pBSK medium (data not shown).

It is generally presumed that spirochetes within unfed midguts are nonmotile (49); we confirmed this by time-lapse confocal imaging at various depths through multiple Bb914-infected, flat

nymphal midguts (Supplemental Video 2). Given the marked differences in both the midgut environment (43, 46) and the metabolic states of spirochetes before and during feeding (50–54), we conjectured that organisms in unfed and fed midguts would differ in their capacities to become motile following exposure to culture medium. To test this idea, unfed midguts immersed in CMRL or BSK-II were nicked and examined by time-lapse epifluorescence microscopy. Nearly all spirochetes attached to the midgut epithelium near the nick site remained nonmotile throughout a 30-minute viewing period (Supplemental Video 3). The few organisms released into the surrounding medium were nonmotile when first observed and exhibited only sluggish motility, at best, after 30 minutes (Supplemental Video 3). Seventy-two-hour-fed mid-

**Figure 5**

Spirochetes advance around and between epithelial cells toward the basement membrane. (A–C) Representative silver-stained paraffin sections and (D–F) FM4-64-labeled cryosections of midguts isolated from Bb914-infected nymphs at (A and D) 48 and (B, C, E, and F) 72 hours after placement on naive C3H/HeJ mice. (F) Digital enlargement of the boxed area in E. Representative examples of differentiated (dc) and undifferentiated cells (uc) are indicated. Arrows indicate spirochete aggregates on the epithelial surface (A–C) or aggregates within the intercellular spaces (D). Asterisks in F indicate organisms in a head-on orientation near the basement membrane. Scale bars: 25  $\mu\text{m}$  (A–E); 5  $\mu\text{m}$  (F).

guts were similarly examined. Unlike what was observed with the nicked, unfed midguts, many of the organisms attached to epithelial cells near the nick site ( $\leq 1.5$  mm) were flexing at their unattached ends as soon as they were imaged (Supplemental Video 4) and became increasingly vigorous over a 30-minute viewing period (data not shown). In contrast to the nonmotile organisms within the lumens of intact, fed midguts (Supplemental Video 1), spirochetes released from the luminal contents (indicated by the presence of blood remnants) into CMRL or BSK-II displayed vigorous motility (Supplemental Video 4). The majority of spirochetes more distal to the nick site (i.e., within the stomach,  $\sim 5$  mm away), however, remained nonmotile (Supplemental Video 4).

*Fed midguts inhibit spirochete motility in a gelatin matrix-based assay.* To clarify the above findings, we devised an experimental system to examine the effect of the midgut environment on spirochete motility. Consistent with the well-documented propensity of spirochetes to localize in collagen-rich tissues (55, 56), we found that a substantial percentage ( $56\% \pm 12\%$ ) of input Bb914 readily penetrated a 5% gelatin matrix and were retained following extensive washing. Organisms within the matrix remained actively motile for at least 6 hours at room temperature. In contrast to BSK-II, in which nearly all organisms displayed translational motility characteristic of *B. burgdorferi* in a low-viscosity milieu (57, 58), spirochetes within the gelatin matrix exhibited 3 distinct motility patterns: motile/translational, motile/nontranslational, and nonmotile (Table 1; see Supplemental Video 5 for representative examples). Installation of a small aliquot (1–2  $\mu\text{l}$ ) of mouse blood into a sample well in a corner of a matrix resulted in a marked and progressive increase in both the overall percentage and degree of motility of the organisms over a 15-minute viewing period; this effect was noticeably less pronounced with increasing distance from the well (Table 1). In stark contrast, the vast majority of spirochetes ( $\sim 92\%$ ) in proximity to the sample well were nonmotile soon after the addition of a naive, 72-hour-fed midgut to the sample well and remained so throughout the entire 15-minute viewing period (Table 1). Contrary to what was observed with blood, the inhibitory effect of the fed midgut diminished as the distance from the well increased (Table 1). Notably, neither unfed midguts

nor salivary glands isolated at 72 hours after placement had any discernible effect on spirochete motility. Trajectory plots depicting the motility patterns of spirochete populations exposed to the various samples in this model system illustrate the contrast between the stimulatory effect of fresh mouse blood and the potent inhibitory effect of 72-hour-fed midguts (Figure 6).

*Penetration of Borrelia into the hemocoel is a rare event.* Spirochetes were not observed in hemolymph until 72 hours after placement (data not shown), suggesting that this time point marks a critical period during which organisms complete the traversal of the midgut. Despite careful examination of the basolateral surfaces of fifty 72-hour-fed midguts, we found only a single spirochete protruding through the basement membrane into the hemocoel (Figure 7A). The ostensible rarity of this event was in accord with the small number of organisms ( $\sim 3$ –4 per tick) observed in isolated hemolymph (Figure 7B) by epifluorescence microscopy and the miniscule number detected by qPCR of hemolymph as compared with fed midguts ( $477 \pm 322$  versus  $5.88 \times 10^6 \pm 1.49 \times 10^5$  genome copies per tick, respectively) at 72 hours after placement. Interestingly, the robust motility of organisms in hemolymph (Supplemental Video 6) was in marked contrast to the lack of motility of spirochetes in intact unfed and fed midguts. Hemocytes containing GFP-positive material, presumably phagocytosed spirochetes, also were visualized in hemolymph (Figure 7C).

*Borrelia attach to all acini types but invade only types II and III.* Staining with FM4-64 allowed unambiguous identification, using established morphologic criteria (43, 59, 60), of all 3 acini types in salivary glands isolated from flat (Figure 8A) as well as fed (Figure 8, B–D) nymphs. In accord with previous reports (43, 59, 60), type I acini, unlike types II and III acini, did not hypertrophy with feeding (Figure 8B). Despite meticulous examination of glands from more than 100 fed nymphs, no spirochetes were observed either on or within acini at 24 or 48 hours after placement (Table 2). By 72 hours, however, spirochetes were observed on the surfaces of all 3 types of acini, albeit in small numbers (Table 2 and Figure 8, B–D). Whereas preferential attachment to a particular acini type was not observed, spirochetes were seen only within types II and III acini (Table 2 and Figure 8, B–D).



**Table 1**  
Inhibition of spirochete motility by fed nymphal midguts in a gelatin matrix-based assay

Experimental sample	Motile/translational <sup>A</sup>	Motile/nontranslational <sup>B</sup>	Nonmotile
BSK-II	95.53 ± 7.47	0 ± 0	4.47 ± 7.47
Gelatin alone	6.81 ± 10.96	51.77 ± 3.48	41.43 ± 3.48
Mouse blood, 0 mm <sup>C</sup>	33.09 ± 18.59	53.29 ± 15.65	13.61 ± 15.65
Mouse blood, 5 mm <sup>C</sup>	15.41 ± 9.50	57.55 ± 18.98	27.04 ± 17.3
Fed midgut, 0 mm <sup>C</sup>	0 ± 0	8.30 ± 13.28	91.70 ± 13.28
Fed midgut, 5 mm <sup>C</sup>	4.97 ± 6.18	68.20 ± 17.43	26.83 ± 19.18
Unfed midgut, 0 mm <sup>C,D</sup>	3.76 ± 3.32	49.46 ± 13.13	46.78 ± 12.59
Salivary glands, 0 mm <sup>C,D</sup>	12.45 ± 9.15	56.44 ± 6.12	31.11 ± 15.07

Values denote mean percentages ± SD calculated using three 5-minute viewing intervals taken over a 15-minute observation period. A minimum of 500 organisms were scored for each sample. Highly similar results were obtained for each sample in 3 independent experiments.

<sup>A</sup>Organisms that exhibited net displacement in the x and/or y axis. <sup>B</sup>Organisms that exhibited obvious signs of motility (i.e., flexing) but no net displacement in either axis. <sup>C</sup>Measurement denotes distance from the well containing the experimental sample. <sup>D</sup>Similar values were obtained at the 5-mm distance (not shown).

**Discussion**

Motility has long been believed to be essential for dissemination of *B. burgdorferi* from the site of inoculation and subsequent invasion of mammalian host tissues (61, 62). The linkage between motility and infectivity for mammals recently was strengthened by intravital imaging of blood-borne spirochetes in mice; following attachment to the vascular endothelium, *B. burgdorferi* move toward and then rapidly penetrate endothelial cell junctions (63, 64). Previous attempts to elucidate the mechanisms of spirochete dissemination within the arthropod have employed fixation and microscopic techniques that preclude analysis of the dynamic interactions between pathogen and vector (19, 20, 37). In this study, we utilized a *B. burgdorferi* transformant harboring a stable, constitutively expressed GFP reporter to track live spirochetes during transmission by *I. scapularis* nymphs. Our investigations revealed, quite unexpectedly, that *Borrelia* progress toward the basement membrane of the midgut as nonmotile aggregates that are closely associated with the epithelial cells. Only well into the feeding process do spirochetes transition to the motile, invasive phenotype in which they conclude their journey within the nymphal tick, infect a mouse, and, ultimately, transit back into a naive vector during larval feeding.

The nymphal midgut undergoes complex physiological and morphological changes during feeding (43, 45, 46). The influx of interstitial fluid during the preparatory phase primes the epithelial cells for nutrient uptake and stimulates activation of the digestive machinery (43, 45, 46). Toward the end of the preparatory phase, midgut epithelial cells begin to secrete components of the peritrophic membrane, a semipermeable layer composed of chitin, proteoglycans, and proteins that protects the epithelium from ingested pathogens and abrasive food particles (65, 66). As feeding progresses, salivary enzymes degrade formed elements in the blood, the remnants of which are avidly phagocytosed and digested to completion within lysosomal food vacuoles (43, 45, 46). The uptake of nutrients promotes the growth and differentiation of epithelial cells, some of which eventually slough from the basement membrane and disintegrate, releasing their contents into the lumen; replacement by adjacent undifferentiated cells maintains the integrity of the epithelial layer (43, 45, 46). Our

results highlight the remarkable degree to which spirochetes accommodate to, and even exploit, this rapidly changing and potentially dangerous milieu. For instance, *B. burgdorferi* escape digestion within the lumen by being situated in the ectoperitrophic space, a protected position presumably attained when spirochetes colonize the midgut at the time of larval acquisition (67). Another example was provided by our observation that spirochetes shed copious blebs at the outset of feeding. The contrast between the avid internalization of blebs by epithelial cells and the exclusively extracellular localization of intact organisms was impressive and suggests that *Borrelia* employ an unknown mechanism to evade uptake and certain destruction while maintaining an intimate association with highly active digestive cells. It is widely believed that the logarithmic expansion of the spirochete population in response to the blood meal

occurs in parallel with the detachment of individual organisms from the luminal surface and their rapid migration through the midgut epithelium (13, 14, 37, 40, 68). We found instead that replicating spirochetes coalesce from scattered foci distributed on and deeply within the epithelium into networks of nonmotile organisms that advance toward the basement membrane by surrounding individual epithelial cells. According to this alternative model, which we call adherence-mediated migration, the strategic positioning of spirochetes at multiple points around individual cells prior to feeding facilitates midgut traversal by enabling the

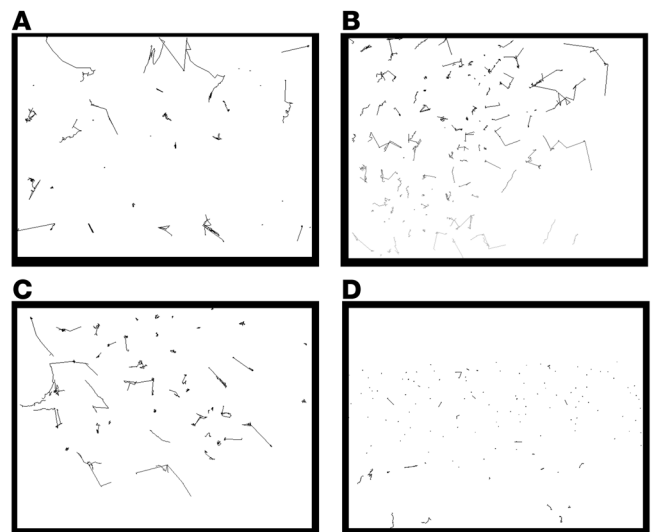


**Figure 6**  
Motility of *B. burgdorferi* in a gelatin matrix model system is inhibited by fed midgut. Trajectory maps showing the motility of *Borrelia* in (A) BSK-II medium, (B) a gelatin matrix alone, (C) a gelatin matrix with a sample well containing fresh mouse blood, and (D) a gelatin matrix with a sample well containing a 72-hour-fed midgut from an uninfected nymph. The trajectory maps were generated from time-lapse epifluorescence images acquired adjacent to the sample well during the first minute of viewing using the MultiTrack plug-in of Image J (95).

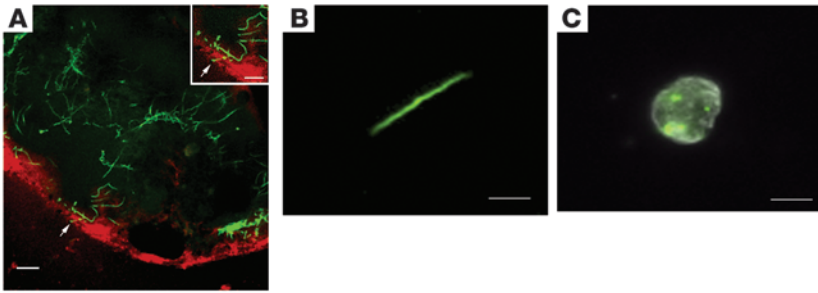


**Figure 7**

Penetration of *B. burgdorferi* into the hemocoel is a rare event. (A) A spirochete (arrow) traversing the basement membrane of an isolated midgut obtained 72 hours after placement on a naive C3H/HeJ mouse. The inset shows a digital enlargement of the penetrating spirochete. (B and C) Representative micrographs of (B) a spirochete and (C) a hemocyte containing GFP-positive material within hemolymph collected 72 hours after placement. Scale bars: 10  $\mu\text{m}$ .

expanding population of *Borrelia* to reach the base of the epithelium faster than the ballooning epithelial cells can transport them toward the lumen. Residual organisms left behind by detaching digestive cells are likely to be ideally situated for penetrating the thinner regions of the epithelium comprised predominantly of undifferentiated cells. It is interesting to note that spirochetal networks are readily discernible, though were not recognized as such, in previously published confocal immunofluorescence micrographs of fed nymphal midguts (14, 24, 68); the significance of network formation most likely was not appreciated in these studies because the specimens were fixed prior to imaging.

It is a central tenet of Lyme disease pathogenesis that *Borrelia* transition between 2 dramatically different transcriptional programs with the onset of tick feeding, with motility being a salient, distinguishing phenotypic trait. Live imaging has revealed that this conception is an oversimplification. That *Borrelia* within unfed nymphal midguts are nonmotile is consistent with the quiescent metabolic state of organisms in this milieu (50–54) and is in line with observations made with crushed midguts dating back to the discovery of the Lyme spirochete as a tick-borne pathogen (49). On the other hand, our finding that the fed midgut is populated with replicating, but nonmotile, spirochetes was unexpected and runs counter to the prevailing notion, which equates metabolic activity with motility (58). Evidence presented herein, however, indicates that the ostensibly identical motility phenotypes in flat and fed ticks are mechanistically distinct. First, we found that spirochetes in unfed midguts displayed, at best, sluggish motility even after prolonged exposure to CMRL or BSK-II, while *Borrelia* in fed midguts became highly active within minutes following exposure to the same medium. Second, in a gel matrix model in which the effect of exogenous substances on spirochete motility could be assessed qualitatively and quantitatively, organisms in proximity to fed, but not flat, midguts rapidly lost motility. To explain these observations, we hypothesize that the physiologic adaptation of spirochetes to the nutritionally deficient milieu of the unfed midgut restricts their capacity to import and/or utilize nutrients needed to power the flagellar motor, whereas the flagellar motors of spirochetes actively replicating within the fed midgut are reversibly disengaged in response to one or more diffusible factors elaborated by the midgut epithelium. Indeed, the lack of motility displayed by spirochetes in the lumens of fed

midguts was remarkable in light of the strong chemoattractant properties of blood in the gel matrix model and other in vitro systems (54, 69). These results, although counterintuitive at first blush, make sense; if blood in the midgut acted as a chemoattractant, spirochetes would never disseminate during feeding. The rapidity of the transition to motility once the midgut environment was breached argues strongly for a posttranscriptional form of control and is consistent with a growing number of reports that bacteria can quickly and reversibly modulate their state and degree of motility via protein-protein interactions involving the flagellar motor and chemosensory apparatus (70, 71).

The midgut epithelium is well recognized as an anatomical barrier to the migration of vector-borne pathogens following ingestion by hematophagous arthropods (4–6). Three complementary lines of evidence suggest that the midgut of *I. scapularis* functions in a similar capacity to impede the dissemination of *B. burgdorferi*. One is the marked reduction in spirochete numbers in the hemolymph relative to the fed midgut; it is noteworthy that the spirochete burdens in hemolymph determined here by qPCR are highly similar to those reported by Coleman et al. (15), who enumerated spirochetes by IFA. A second comes from our micrographs, which revealed a tapering in the density of networks toward the basolateral pole of the epithelium, where some spirochetes were wedged between cells, assuming a head-on orientation. The last was the rarity of actually observing spirochetes “caught in the act” of penetrating through the midgut into the hemocoel. Contrary to an earlier report (40), we did not find any evidence for the intracellularity of intact spirochetes as they traverse the midgut. Our results imply that the intercellular junctions and basement membrane form a series of anatomical barriers that *Borrelia* must cross in order to gain access to the hemocoel. A key prediction of our model is that adherence-mediated migration positions spirochetes in proximity to the intercellular junctions as they become weakened by remodeling and the basement membrane is thinned by luminal distention (43, 45, 46). Negotiation of these structural impediments presumably requires the resumption of motility and is likely facilitated by the binding of host-derived molecules, such as plasminogen, to the bacterial surface (15, 16). Conceivably, chemoattractants originating from the hemocoel and/or stimuli resulting from the interaction of spirochetes with midgut components at or near the intercellular junctions override the inhibitory factor(s) secreted by the midgut epithelium. While the factors and environmental cues promoting the transition to motility remain to be determined, it is important to note that the motile phenotype consistently displayed by organisms within the hemolymph is a biophysical necessity for translation within the fluid-filled hemocoel (58, 72). This point in the dissemination process, therefore, can be thought of as marking the convergence of our model with in vitro (73, 74) and in vivo (63, 64) studies depicting highly motile organisms penetrating cellular junctions and extracellular matrices.

The miniscule numbers of organisms observed on and within salivary glands is in line with reports by others (18, 19, 29, 33) and is consistent with studies indicating that mammalian infection is initiated by a small inoculum of highly virulent organisms delivered to the feeding site (31, 75). Undoubtedly, the paucity of gland-

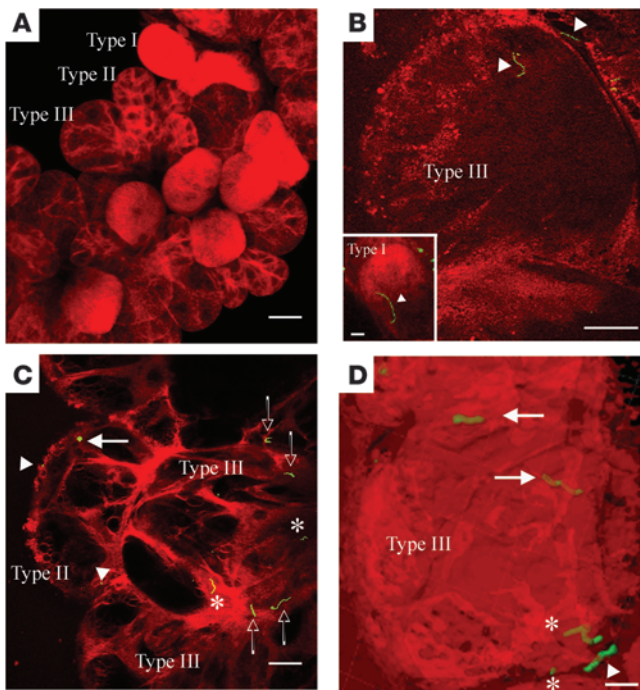


**Figure 8**

*B. burgdorferi* are present on salivary glands in low numbers and are observed only within types II and III acini. Representative micrographs of salivary glands isolated from (A) flat or (B–D) fed nymphs at 72 hours after placement on C3H/HeJ mice. Spirochetes (arrowheads) adhering to the surfaces of (B) type III acini and type I (inset). (C) Representative 10- $\mu$ m composite confocal image showing spirochetes on the surfaces of and within types II and III acini. Spirochetes on the surface (arrowheads), below the surface near the basement membrane (filled arrows), between epithelial cells (open arrows), and within ducts (asterisks) are indicated. (D) Single view taken from a 3D reconstruction showing spirochetes on the surface of (arrowheads), penetrating into (asterisks), and within (arrows) a type III acinus. Note the size difference between type I acini (B, inset), which do not hypertrophy, and the hypertrophied types II and III acini in B–D. Scale bars: 25  $\mu$ m (A–D); 5  $\mu$ m (B, inset).

associated spirochetes reflects, at least in part, the small percentage of organisms that successfully penetrate the midgut and enter the hemolymph. Although *I. scapularis* hemolymph is poorly borreliacidal (76), elimination of spirochetes by cellular innate defenses within the hemocoel, shown herein by us and others (15), may further limit the number of organisms that reach their salivary gland target. Because salivary glands are a well-recognized anatomical barrier for vector-borne pathogens (6, 77–79), it is also plausible that this organ impedes the migration of *B. burgdorferi*. Along these lines, our visualization of spirochetes in association with the acinar surface as well as with multiple intraglandular structures raises the possibility that, as postulated for the midgut, the salivary glands comprise a succession of obstacles that the spirochete must negotiate via a multistep process in order to attain its goal of accessing the salivary stream. The similar time frames at which spirochetes are detected in the salivary glands and are transmitted to murine tissue, 72 hours here and 60 hours in the extensive time-course analyses conducted by Ohnishi et al. (31), suggest that motile *Borrelia* are adept at surmounting these glandular barriers efficiently. Interestingly, although similar numbers of organisms

were observed on the surfaces of all 3 types of acini, implying equal distribution of receptors or attachment sites around the glands, we observed spirochetes only within types II and III acini. The absence of organisms within type I acini, which do not undergo hypertrophy and remodeling during feeding (43, 59, 60), suggests that thinning of the acinar basement membrane may be integral to the spirochete’s strategy for penetration of salivary glands. Invasion of types II and III acini also may be driven by chemotactic factors that are not produced by type I acini (80).

The transcriptional and translational changes that the Lyme disease spirochete undergoes in response to mammalian host- and arthropod-derived signals have been the subject of intensive investigation (12, 21, 23, 24). Abundant evidence has emerged indicating that the Rrp2/RpoN/RpoS pathway serves as a master regulator of the genetic programs required for infection of the mammalian host (19, 35, 51, 81–83). The imaging studies presented here provide a structural framework for interpreting the transcriptional events mediated by RpoS during tick-to-mammal transmission. For example, we (35) and others (31, 44) have demonstrated that the majority of spirochetes within fed nymphal midguts continue to express substantial amounts of both *ospA* transcript and protein throughout the blood meal. Our model for adherence-mediated migration holds that the protracted down-regulation of *ospA* mediated by RpoS (51) would maintain spirochetes in close contact with epithelial cells via interaction with TrospA (37), and possibly other surface receptors, until the midgut barriers weaken. Among those genes upregulated by RpoS in vivo (51), 4 (*cheW-2*, *mcp1*, *mcp4*, and *mcp5*) encode proteins related to chemotaxis (84), and a fifth (*oppA5*) may be involved in nutrient sensing (85); expression of one or more of these genes may be

**Table 2**

Attachment to and invasion of salivary gland acini by *B. burgdorferi*

Time after placement	Acini with surface-associated <i>Bb</i> <sup>A</sup>			Acini containing <i>Bb</i> <sup>B</sup>			Total acini positive for <i>Bb</i>
	Type I	Type II	Type III	Type I	Type II	Type III	
0 h	0 (19)	0 (21)	0 (20)	0 (19)	0 (21)	0 (19)	0 (60)
24 h	0 (14)	0 (21)	0 (19)	0 (14)	0 (21)	0 (19)	0 (54)
48 h	0 (12)	0 (53)	0 (40)	0 (12)	0 (53)	0 (40)	0 (105)
72 h	3 (43)	4 (49)	7 (93)	0 (43)	8 (49) <sup>C</sup>	11 (93) <sup>D</sup>	33 (185)

Values denote number of acini (total examined). <sup>A</sup>Acini with surface-associated spirochetes following multiple washes. <sup>B</sup>Acini containing spirochetes near the basement membrane, between epithelial cells, or within acinar ducts. <sup>C</sup>*P* < 0.01; <sup>D</sup>*P* < 0.003 vs. type I.



critical for the transition from the nonmotile to motile phenotype of organisms that penetrate the hemocoel. The complexity of the spirochete's RpoS-dependent, as well as RpoS-independent, regulatory networks results in an extraordinary degree of transcriptional and antigenic heterogeneity within the feeding midgut (29, 31, 35, 44, 86). A key question for future investigations is whether *Borrelia* reach the hemocoel as a result of a purely stochastic process dependent on the deposition of large numbers of organisms near the basement membrane or by selection for spirochetes expressing an "invasion-competent" transcriptional profile.

## Methods

**B. burgdorferi strains, culture conditions, and growth curves.** CE162, a virulent clonal derivative of strain *B. burgdorferi* 297 (32), CE863, a CE162 transformant harboring *P<sub>flaB</sub>-gfp* on a cp32-derived shuttle vector (34), and Bb914, described below, were cultivated in BSK-II medium (87) supplemented with 6% normal rabbit serum (Pel-Freez Biologicals). Bb914 and CE863 were grown in the presence of gentamycin (50 µg/ml) and kanamycin (400 µg/ml), respectively. Borrelial cultures were passaged no more than 3 times prior to experimental manipulations. The plasmid content of each isolate was monitored by PCR as previously described (88). To obtain temperature-shifted organisms, *B. burgdorferi* clones were grown at 23°C to a density of 2 to 5 × 10<sup>6</sup> spirochetes/ml, diluted into fresh BSK-II to a density of 1 × 10<sup>3</sup> spirochetes/ml, and incubated at 37°C until mid-log phase (~5 × 10<sup>7</sup> spirochetes/ml). For determination of growth curves following temperature shift, spirochetes were enumerated over 10–12 days by dark-field microscopy with a Petroff Hausser counting chamber (Hausser Scientific); growth curves for each isolate were performed in triplicate in at least 3 independent trials. Mammalian host-adapted spirochetes were obtained by cultivation of organisms in DMCs implanted into the peritoneal cavities of rats as previously described (89).

**Generation of Bb914.** The strategy used to generate pMC1916, a suicide vector for insertion of a constitutively expressed *P<sub>flaB</sub>-gfp* reporter and a gentamycin-resistance cassette into the endogenous cp26 plasmid of strain 297, is presented in Supplemental Figure 1A (see Supplemental Table 1 for primers). First, approximately 1 kb each of the upstream and downstream sequences flanking the *bbb20-bbb21* intergenic region were amplified from CE162. The resulting upstream and downstream region amplicons were separately cloned into pCR2.1-TOPO (Invitrogen), yielding plasmids pMC1624 and pMC1626, respectively. The cp26 "crossover region" was generated by ligating the insert from pMC1626 into linearized pMC1624, both digested with *AatII* and *XhoI*, yielding plasmid pMC1636. To facilitate subsequent cloning steps, the cp26 crossover region was subcloned out of pMC1636 by digestion with *BssHIII* and ligated into similarly digested pBluescript II (Stratagene), yielding plasmid pMC1661. The polylinker from the pBluescript II SK vector was amplified using primers containing *AatII* restriction enzyme sites and then subcloned into *AatII*-digested pMC1661, yielding plasmid pMC1667. GFP under the control of the borrelial *flaB* promoter was subcloned from *P<sub>flaB</sub>-gfp*/pCE320 (88) by digestion with *XhoI* and *XbaI* and ligated into similarly digested pMC1667. A fragment containing *P<sub>flaB</sub>-aacC1*, encoding resistance to gentamycin, was amplified from pBSV2G (90) using primers containing flanking *SacI* restriction enzyme sites and cloned into *SacI*-digested pMC1667, yielding the final suicide plasmid construct, pMC1916. Orientations of the *P<sub>flaB</sub>-aacC1* and *P<sub>flaB</sub>-gfp* cassettes within pMC1916 were confirmed by sequencing, using primers BBB20 junc F and BBB21 junc R, respectively. Competent CE162, prepared using the method described by Samuels et al. (91), was electroporated with approximately 20–30 µg of CsCl-purified pMC1916; transformants were selected in 96-well plates in BSK-II containing gentamycin (83). Supplemental Figure 1B depicts the double-crossover event between

pMC1916 and the endogenous cp26, which resulted in Bb914. Insertion and orientation of the *P<sub>flaB</sub>-aacC1* and *P<sub>flaB</sub>-gfp* cassettes in Bb914 were confirmed by PCR using primer pairs BBB20ups 5'-BssHIII plus flgB-aacC1 3'-*SacI* and BBB22downs 5'-BssHII plus GFP601-R, respectively.

**Effect of FM4-64 on spirochete motility and viability.** One ml aliquots of Bb914, cultured to mid-log phase (~5 × 10<sup>7</sup> spirochetes/ml) following temperature shift, were incubated for 24 hours at 37°C in BSK-II in the absence or presence of graded concentrations (2 ng/ml to 100 µg/ml) of FM4-64 (Invitrogen). Following incubation, organisms were assessed for motility by dark-field microscopy and for viability by solid-phase plating in pBSK (91).

**SDS-PAGE.** Cultures of Bb914 and CE162, before and after temperature shift and following cultivation within DMCs, were harvested by centrifugation at 8,000 g for 15 minutes at 4°C, and the resulting pellets were washed twice with PBS. Whole-cell lysates from 1 × 10<sup>7</sup> organisms were boiled in Laemmli sample buffer (Bio-Rad), separated in 12.5% SDS-polyacrylamide gels, and stained with silver as previously described (32).

**Flow cytometry.** *B. burgdorferi* strains Bb914 and CE863, grown to mid-log phase following temperature shift, were analyzed on a FACSCalibur flow cytometer (BD) as previously described (92). In brief, *B. burgdorferi* cells were stained with the nucleic acid stain SYTO59 (Invitrogen) before fixation in 1% paraformaldehyde in FA buffer (Difco). For each sample, data were collected for 100,000 SYTO59 positive events and analyzed using WinMidi (version 2.8). Three independent experiments were performed for each construct and condition.

**Determination of ID<sub>50</sub> values for CE162 and Bb914.** Groups of five 3- to 5-week-old female C3H/HeJ mice (Jackson Laboratories) were inoculated intradermally with 1 × 10<sup>2</sup>, 1 × 10<sup>3</sup>, or 1 × 10<sup>4</sup> temperature-shifted Bb914 or CE162. Infection was assessed at 4 weeks after inoculation by cultivation of ears, joints, hearts, and bladders in BSK-II containing *Borrelia* antibiotic cocktail (Sigma-Aldrich). The percentage of infected animals in each group was used to determine the ID<sub>50</sub> values using ID50 software, available from the NIH ([ftp://ftp.ncbi.nih.gov/pub/spouge/web/software/ID50\\_5.0\\_Windows](ftp://ftp.ncbi.nih.gov/pub/spouge/web/software/ID50_5.0_Windows)), as previously described (93, 94). All experimental procedures using mice were approved by and performed in accordance with the guidelines of the University of Connecticut Health Center Institutional Animal Care and Use Committee.

**Tick acquisition and transmission of *B. burgdorferi*. I. scapularis** larvae (Department of Entomology, Oklahoma State University) and nymphs were stored in an incubator at 22°C over saturated potassium sulfate (95%–97% relative humidity) with a 16-hour light/8-hour dark cycle. Naive larvae were fed to repletion on BALB/c SCID or C3H/HeJ mice (Jackson Laboratories) 2 weeks after syringe inoculation with either Bb914 or CE162 (1 × 10<sup>4</sup> spirochetes). Engorged larvae were crushed into 10 µl of PBS for examination by epifluorescence microscopy (GFP filter-475/510 nm), processed for qPCR (see below), or allowed to molt into nymphs. For all transmission experiments, flat nymphs infected with Bb914 or CE162 were fed on naive C3H/HeJ mice and processed for microscopy or qPCR as described below; murine infection was confirmed at 4 weeks by cultivation of ears, joints, hearts, and bladders in BSK-II. Nymphs used in these experiments typically attached and established a feeding site within the first 24 hours following placement on mice and were replete by 96–108 hours. Because the actual time of attachment for individual ticks varies, hours indicated are after placement.

**Analysis of *OspC* expression in Bb914-infected ticks by IFA.** Expression of *OspC* and FlaB within flat nymphs and nymphs fed for 72 hours on naive mice was determined by double-label indirect immunofluorescence using polyclonal, monospecific rat and rabbit anti-serum directed against *OspC* and FlaB, respectively, as previously described (35). Midguts were mounted in Vectashield (Vector Laboratories) and viewed on a BX41 epifluorescence microscope (Olympus) equipped with FITC and rhodamine



filters,  $\times 40$  (0.65 numerical aperture [NA]) objective, and a Retiga EXi CCD camera (Q Imaging). All epifluorescence images (here and below) were acquired at  $696 \times 520$  pixel resolution. At least 7 unfed and 7 fed nymphs each were examined. The mean percentage ( $\pm$  SD) of OspC labeling was calculated based on the number of FlaB-labeled organisms.

**Enumeration of spirochetes by qPCR.** DNA was isolated from engorged larvae (pools of 10), unfed nymphs (pools of 15), and replete nymphs (pools of 5) using the Puregene Yeast/Bact. Kit B (QIAGEN) according to the manufacturer's instructions. Spirochete burdens within infected ticks were assessed using a TaqMan assay directed against *flaB* (*bb0147*; Supplemental Table 1) performed using iQ SuperMix (Bio-Rad) in an iCycler thermal cycler (Bio-Rad). Purified plasmid DNA containing the target gene amplicon cloned into pCR2.1 TOPO (Invitrogen) was used to generate a standard curve ( $10^7$ – $10^2$  copies/ $\mu$ l). For each experiment, the standard curve and negative controls were analyzed in duplicate, whereas experimental samples were analyzed in quadruplicate. Copies of *flaB* present in each sample were calculated using the iCycler post-run analysis software (version 3.1) based on internal standard curves. The means ( $\pm$  SD) for each stage were derived from 3 independent pools.

**Confocal microscopy to determine the distribution of live Bb914 within freshly isolated, nymphal midguts and salivary glands.** Bb914-infected flat nymphs and infected nymphs removed from naive C3H/HeJ mice at 24, 48, or 72 hours after placement were decapitated using a no. 11 scalpel blade and placed on a microscope slide containing 10  $\mu$ l of CMRL or BSK-II. Midguts then were carefully dissected from the cuticle; specimens showing gross evidence of disruption (i.e., visible leakage of luminal contents) were discarded. Isolated midguts then were transferred to a clean microscope slide and immersed in CMRL or BSK-II containing FM4-64 (2 ng/ml). The tip of a single diverticulum was gently nicked with a no. 11 scalpel and the entire midgut was incubated for 3 minutes at room temperature to allow for uptake of the dye. The midguts were gently washed 3 times with CMRL or BSK-II to remove unbound FM4-64 and transferred to a clean microscope slide containing a drop of Vectashield (Vector Labs). Specimens were viewed on a LSM-510 confocal microscope (Zeiss) equipped with argon and HeNe lasers using a  $\times 40$  (1.3 NA) oil-immersion objective within 20 minutes of sample preparation. Optical sections were acquired at 1- $\mu$ m intervals through the full thickness of midguts isolated from flat and fed nymphs 24 and 48 hours after placement. The large amount of blood combined with the marked expansion of the luminal space, however, precluded imaging through the full thickness ( $>90$   $\mu$ m) of midguts isolated at 72 hours after placement. Consequently, individual diverticula from 72-hour-fed midguts were incised gently to expose the lumen, and optical sections were acquired from the luminal surface toward the basement membrane. All images were acquired at  $512 \times 512$  pixel resolution and analyzed using ImageJ (95). Composite images, here and elsewhere, comprise serial Z-series images collected in both red and green channels. A minimum of 20 nymphal midguts were examined for each time point.

Intact salivary glands were carefully dissected from the same cohort of ticks used to obtain midguts and immersed in CMRL or BSK-II containing FM4-64 (2 ng/ml) for 3 minutes at room temperature. The glands then were gently washed 3 times with CMRL or BSK-II to remove unbound FM4-64 and transferred to a clean microscope slide containing a drop of Vectashield; glands were examined within 20 minutes of specimen preparation. Confocal microscopy and image analysis were performed as described above for midguts. A minimum of 20 pairs of salivary glands were examined for each time point. Three-dimensional reconstructions of salivary glands were generated using IMARIS (Bitplane AG) imaging software.

**Time-lapse confocal imaging of live spirochetes within freshly isolated, intact midguts.** Midguts from Bb914-infected flat nymphs and infected nymphs forcibly removed from naive C3H/HeJ mice at 48 and 72 hours after placement

were carefully dissected as above and immersed in CMRL or BSK-II containing FM4-64; for these experiments, specimens were not nicked. After 3 minutes of incubation, the midguts were washed gently 3 times with CMRL or BSK-II to remove unbound FM4-64, transferred to clean, dry microscope slides, and mounted in Vectashield, immersion oil, CMRL, or BSK-II. Confocal microscopy was performed as described above using a  $\times 63$  (1.4 NA) oil-immersion objective; only those midgut specimens that excluded FM4-64 were considered to be intact and used for time-lapse imaging. Images ( $512 \times 512$  pixel resolution) were acquired at 1-minute intervals for a total of 1.5 hours. A minimum of 7 intact midguts were examined for each time point. Image analysis was performed using ImageJ (95) and QuickTime Pro (Apple) software.

**Time-lapse epifluorescence imaging of live spirochetes within freshly isolated, intact, and nicked midguts.** To assess the motility of spirochetes within the undisturbed midgut environment, midguts from Bb914-infected flat nymphs and infected nymphs forcibly removed from naive C3H/HeJ mice at 72 hours after placement were carefully dissected and immersed, without nicking, in CMRL or BSK-II containing FM4-64. After 3 minutes of incubation, the midguts were washed gently 3 times with CMRL or BSK-II to remove unbound FM4-64, transferred to clean, dry microscope slides, mounted in CMRL or BSK-II, and viewed on a BX41 epifluorescence microscope using a  $\times 40$  (1.3 NA) oil-immersion objective; only specimens that excluded FM4-64 were used for time-lapse imaging. Images ( $696 \times 520$  pixel resolution) were acquired using a Retiga EXi CCD camera at 5-minute intervals for a total of 30 minutes. Image analysis was performed using ImageJ (95) and QuickTime Pro (Apple) software. A minimum of 7 unfed and 7 fed midguts were examined in either CMRL or BSK-II.

To assess the effect of a breach in the midgut environment on spirochete motility, midguts from Bb914-infected flat nymphs and 72-hour-fed nymphs were carefully dissected and immersed in CMRL or BSK-II. The tip of a diverticulum was nicked with a no. 11 scalpel to expose spirochetes to culture medium, a cover glass was applied, and the specimen was viewed on a BX41 microscope using a  $\times 40$  (1.3 NA) oil-immersion objective. Images ( $696 \times 520$  pixel resolution) were acquired using a Retiga EXi CCD camera at 5-minute intervals for a total of 30 minutes. The distance of spirochetes from the nick site was determined using an optical reticle (Olympus). Image analysis was performed using ImageJ (95) and QuickTime Pro (Apple) software. A minimum of 10 unfed and 10 fed midguts were examined in either CMRL or BSK-II.

**Gelatin matrix-based assay for spirochete motility.** Gelatin matrices ( $\sim 1$  mm thick) were prepared by adding type A gelatin from porcine skin (5% w/v; Sigma-Aldrich) to prewarmed ( $56^\circ\text{C}$ ) PBS. 200  $\mu$ l of the liquefied gelatin solution was added to each chamber of a clean 8-well chamber slide (Lab-Tek). The slides were cured overnight at  $4^\circ\text{C}$  in a humidified chamber and warmed to room temperature prior to use. 150- $\mu$ l aliquots of BSK-II containing approximately  $5 \times 10^7$  in vitro-cultivated Bb914 (harvested during logarithmic phase of growth) were added to each chamber, and the slides were incubated for 1 hour at room temperature. The residual medium was gently removed and saved for the enumeration of organisms that did not penetrate or attach to the matrices. Each chamber subsequently was rinsed 3 times with sterile PBS to remove any loosely bound spirochetes. A well ( $\sim 1$  mm diameter) was gently introduced into one corner of each matrix using a glass pipette, and the chambers were washed 3 times with sterile PBS. Each matrix then was gently separated from its plastic chamber using a sterile scalpel and transferred to a new microscope slide. The wells were filled with approximately 1–2  $\mu$ l of one of the following materials: (a) whole blood, freshly isolated from an uninfected C3H/HeJ mouse; (b) minced midgut from a flat, uninfected nymph; (c) minced midgut from an uninfected nymph 72 hours after placement; or (d) salivary glands isolated from an uninfected nymph 72 hours after



placement. Individual matrices then were covered with a cover glass and viewed on a BX41 epifluorescence microscope using a  $\times 40$  (1.3 NA) oil-immersion objective. For each sample, images ( $696 \times 520$  pixel resolution) were acquired using a Retiga EXi CCD camera at 5-minute intervals immediately adjacent to (0 mm) and 5 mm away from the periphery of the sample well, for a total of 15 minutes at each distance. Individual spirochetes within a given field of view were scored visually as nonmotile, motile/nontranslational (i.e., movement with no net displacement in the  $x$ - $y$  axis), or motile/translational (i.e., movement with net displacement in the  $x$  and/or  $y$  axes) (see Supplemental Video 5 for examples). For each sample, a minimum of 500 spirochetes at the 0 and 5 mm distances were categorized; the percentage of spirochetes in each category represents the average of three 5-minute viewing intervals taken over the 15-minute observation period for each distance. A minimum of 3 experiments were performed for each sample. The  $x$ - $y$  trajectory plots were generated from time-lapse epifluorescence images during the first minute of viewing using the Multi-Track plug-in of ImageJ (95) software.

**Paraffin embedding and silver staining of nymphal midguts.** Bb914-infected nymphs were placed on naive C3H/HeJ mice and then forcibly removed at 48 and 72 hours after placement. Intact midguts were dissected from the cuticle as described above and fixed overnight at  $4^\circ\text{C}$  in 4% paraformaldehyde (pH 7.4) containing FM4-64 (2 ng/ml). Specimens then were briefly rinsed with PBS and embedded in 1% agarose. Once solidified, excess agarose was trimmed, and the samples were placed into histology cassettes (Shandon Lipshaw). Following dehydration in ethanol, the samples were rinsed in toluene and embedded in paraffin. 10- $\mu\text{m}$  sections were stained using the Warthin-Starry procedure (96) and viewed on a BX41 epifluorescence microscope using a  $\times 40$  (1.3 NA) oil-immersion objective. Images were acquired using a Retiga EXi CCD camera at  $696 \times 520$  pixel resolution and analyzed using ImageJ (95).

**Cryosectioning of nymphal midguts.** Bb914-infected nymphs were placed on naive C3H/HeJ mice and then forcibly removed at 48 and 72 hours after placement. Intact midguts were dissected from the cuticle as described above and fixed overnight at  $4^\circ\text{C}$  in 4% paraformaldehyde (pH 7.4) containing FM4-64 (2 ng/ml). The following day, midguts were washed in PBS, soaked overnight at  $4^\circ\text{C}$  in 30% sucrose, and then gently placed in Cryomatrix freezing compound (Thermo Shandon). Five- $\mu\text{m}$  cryosections were cut on a Leica SM1900 Cryostat (Leica) equipped with a CryoJane Frozen Sectioning Kit (Instrumedics Inc.) (97). Images were acquired on a LSM-510 confocal microscope using a  $\times 40$  (1.3 NA) oil-immersion objective at  $512 \times 512$  pixel resolution and analyzed using ImageJ (95).

**Collection of hemolymph.** Bb914-infected nymphs, forcibly removed from naive C3H/HeJ mice at 24, 48, and 72 hours after placement, were surface sterilized by successive washes in sterile water, 0.5% bleach, and 70% ethanol.

The front legs were amputated at the distal joints, and the exuded fluid was collected onto a clean, dry microscope slide as previously described (98). Hemolymph was inspected for contamination with blood and/or midgut material by widefield microscopy prior to being imaged by confocal microscopy. The motility of spirochetes within hemolymph was followed over time on a LSM-510 confocal microscope using a  $\times 63$  (1.4 NA) oil-immersion objective. Time-lapse images ( $512 \times 512$  pixel resolution) were acquired at 5-second intervals for a minimum of 3 minutes per specimen and analyzed using ImageJ (95). To assess spirochete burdens within hemolymph, 15 nymphs were placed in a sterile microfuge tube immediately after the legs were severed at the distal joints and then centrifuged at  $8000\text{ g}$  for 5 minutes to collect the hemolymph. A small aliquot of the hemolymph (0.5  $\mu\text{l}$ ) was removed and examined by widefield microscopy for the presence of blood and/or midgut contaminants. The remaining hemolymph ( $\sim 4\ \mu\text{l}$ ) was transferred into a sterile microfuge tube for qPCR as described above.

**Statistics.** The statistical significance of the quantitative differences between flow cytometric sample groups,  $\text{ID}_{50}$  calculations, and the localization of spirochetes in salivary gland acini was determined by unpaired Student's  $t$  test with 2-tailed  $P$  values using Prism (version 5; GraphPad software).  $P$  values of less than 0.05 were considered statistically significant.

## Acknowledgments

We would like to thank Cynthia Gonzalez for her superb technical assistance, David Rowe and Yaling Liu (Center for Regenerative Medicine and Skeletal Development, University of Connecticut Health Center) for the use of their cryostat, and Nancy Ryan (Research Histology Core Facility, University of Connecticut Health Center) for her assistance with paraffin embedding and silver staining of midguts. We are especially grateful to Daniel Sonenshine (Old Dominion University, Norfolk, Virginia, USA) for sharing his expertise on the physiology of tick feeding and for his critical reading of the manuscript. This work was supported by a National Research Fund for Tick-Borne Diseases grant awarded to M.J. Caimano and by NIH grants AI-29735 (to J.D. Radolf and M.J. Caimano), AR-055323 (to U. Pal), AI-080615 (to U. Pal), and GM-072004 (to C.W. Wolgemuth).

Received for publication April 1, 2009, and accepted in revised form September 30, 2009.

Address correspondence to: Justin D. Radolf, Department of Medicine, University of Connecticut Health Center, 263 Farmington Avenue, Farmington, Connecticut 06030-3715, USA. Phone: (860) 679-8480; Fax: (860) 679-1358; E-mail: jradolf@up.uconn.edu.

1. WHO. 2008. World health statistics. <http://www.who.int/whosis/whostat/2008/en/index.html>.
2. Hill, C.A., Kafatos, F.C., Stansfield, S.K., and Collins, F.H. 2005. Arthropod-borne diseases: vector control in the genomics era. *Nat. Rev. Microbiol.* **3**:262–268.
3. Hemingway, J., Beaty, B.J., Rowland, M., Scott, T.W., and Sharp, B.L. 2006. The Innovative Vector Control Consortium: improved control of mosquito-borne diseases. *Trends Parasitol.* **22**:308–312.
4. Sacks, D., and Kamhawi, S. 2001. Molecular aspects of parasite-vector and vector-host interactions in leishmaniasis. *Annu. Rev. Microbiol.* **55**:453–483.
5. Barillas-Mury, C., and Kumar, S. 2005. *Plasmodium*-mosquito interactions: a tale of dangerous liaisons. *Cell Microbiol.* **7**:1539–1545.
6. Roditi, I., and Lehane, M.J. 2008. Interactions between *trypanosomes* and *tsetse* flies. *Curr. Opin. Microbiol.* **11**:345–351.
7. Baldrige, G.D., et al. 2007. Infection of *Ixodes scapularis* ticks with *Rickettsia monacensis* expressing green fluorescent protein: a model system. *J. Invertebr. Pathol.* **94**:163–174.
8. Vlachou, D., et al. 2004. Real-time, in vivo analysis of malaria ookinete locomotion and mosquito midgut invasion. *Cell Microbiol.* **6**:671–685.
9. Guevara, P., et al. 2005. Expression of fluorescent genes in *Trypanosoma cruzi* and *Trypanosoma rangeli* (Kinetoplastida: Trypanosomatidae): its application to parasite-vector biology. *J. Med. Entomol.* **42**:48–56.
10. Bacon, R.M. 2007. Lyme disease--United States, 2003–2005. *MMWR Morb. Mortal. Wkly. Rep.* **56**:573–576.
11. Steere, A.C., Coburn, J., and Glickstein, L. 2004. The emergence of Lyme disease. *J. Clin. Invest.* **113**:1093–1101.
12. Tilly, K., Rosa, P.A., and Stewart, P.E. 2008. Biology of infection with *Borrelia burgdorferi*. *Infect. Dis. Clin. North Am.* **22**:217–234.
13. Piesman, J., Oliver, J.R., and Sinsky, R.J. 1990. Growth kinetics of the Lyme disease spirochete (*Borrelia burgdorferi*) in vector ticks (*Ixodes dammini*). *Am. J. Trop. Med. Hyg.* **42**:352–357.
14. de Silva, A.M., and Fikrig, E. 1995. Growth and migration of *Borrelia burgdorferi* in *Ixodes* ticks during blood feeding. *Am. J. Trop. Med. Hyg.* **53**:397–404.
15. Coleman, J.L., et al. 1997. Plasminogen is required for efficient dissemination of *B. burgdorferi* in ticks and for enhancement of spirochetemia in mice. *Cell.* **89**:1111–1119.
16. Klempner, M.S., et al. 1995. Binding of human plasminogen and urokinase-type plasminogen activator to the Lyme disease spirochete, *Borrelia burgdorferi*. *J. Infect. Dis.* **171**:1258–1265.
17. Sonenshine, D.E., and Hynes, W.L. 2008. Molecular characterization and related aspects of the innate immune response in ticks. *Front Biosci.* **13**:7046–7063.
18. Ribeiro, J.M., Mather, T.N., Piesman, J., and Spiel-



man, A. 1987. Dissemination and salivary delivery of Lyme disease spirochetes in vector ticks (Acari: Ixodidae). *J. Med. Entomol.* **24**:201–205.

19. Fisher, M.A., et al. 2005. *Borrelia burgdorferi*  $\sigma^{54}$  is required for mammalian infection and vector transmission but not for tick colonization. *Proc. Natl. Acad. Sci. U. S. A.* **102**:5162–5167.

20. Pal, U., et al. 2004. OspC facilitates *Borrelia burgdorferi* invasion of *Ixodes scapularis* salivary glands. *J. Clin. Invest.* **113**:220–230.

21. Stevenson, B., et al. 2006. Evolving models of Lyme disease spirochete gene regulation. *Wien. Klin. Wochenschr.* **118**:643–652.

22. Hojgaard, A., Eisen, R.J., and Piesman, J. 2008. Transmission dynamics of *Borrelia burgdorferi* s.s. during the key third day of feeding by nymphal *Ixodes scapularis* (Acari: Ixodidae). *J. Med. Entomol.* **45**:732–736.

23. Hovius, J.W., van Dam, A.P., and Fikrig, E. 2007. Tick-host-pathogen interactions in Lyme borreliosis. *Trends Parasitol.* **23**:434–438.

24. Pal, U., and Fikrig, E. 2003. Adaptation of *Borrelia burgdorferi* in the vector and vertebrate host. *Microbes Infect.* **5**:659–666.

25. Caimano, M.J., Eggers, C.H., Gonzalez, C.A., and Radolf, J. D. 2005. Alternate sigma factor RpoS is required for the in vivo-specific repression of *Borrelia burgdorferi* plasmid lp54-borne *ospA* and *lp6.6* genes. *J. Bacteriol.* **187**:7845–7852.

26. Tilly, K., et al. 2006. *Borrelia burgdorferi* OspC protein required exclusively in a crucial early stage of mammalian infection. *Infect. Immun.* **74**:3554–3564.

27. Byram, R., Stewart, P.E., and Rosa, P. 2004. The essential nature of the ubiquitous 26-kilobase circular replicon of *Borrelia burgdorferi*. *J. Bacteriol.* **186**:3561–3569.

28. Casjens, S., et al. 2000. A bacterial genome in flux: the twelve linear and nine circular extrachromosomal DNAs in an infectious isolate of the Lyme disease spirochete *Borrelia burgdorferi*. *Mol. Microbiol.* **35**:490–516.

29. Piesman, J., and Schneider, B.S. 2002. Dynamic changes in Lyme disease spirochetes during transmission by nymphal ticks. *Exp. Appl. Acarol.* **28**:141–145.

30. Piesman, J., Schneider, B.S., and Zeidner, N.S. 2001. Use of quantitative PCR to measure density of *Borrelia burgdorferi* in the midgut and salivary glands of feeding tick vectors. *J. Clin. Microbiol.* **39**:4145–4148.

31. Ohnishi, J., Piesman, J., and de Silva, A.M. 2001. Antigenic and genetic heterogeneity of *Borrelia burgdorferi* populations transmitted by ticks. *Proc. Natl. Acad. Sci. U. S. A.* **98**:670–675.

32. Caimano, M.J., Eggers, C.H., Hazlett, K.R., and Radolf, J.D. 2004. RpoS is not central to the general stress response in *Borrelia burgdorferi* but does control expression of one or more essential virulence determinants. *Infect. Immun.* **72**:6433–6445.

33. Grimm, D., et al. 2004. Outer-surface protein C of the Lyme disease spirochete: A protein induced in ticks for infection of mammals. *Proc. Natl. Acad. Sci. U. S. A.* **101**:3142–3147.

34. Eggers, C.H., Caimano, M.J., and Radolf, J.D. 2006. Sigma factor selectivity in *Borrelia burgdorferi*: RpoS recognition of the *ospE/ospF/elp* promoters is dependent on the sequence of the -10 region. *Mol. Microbiol.* **59**:1859–1875.

35. Mulay, V.B., et al. 2009. *Borrelia burgdorferi* *bba74* is expressed exclusively during tick feeding and is regulated by both arthropod- and mammalian host-specific signals. *J. Bacteriol.* **191**:2783–2794.

36. Hammer, B., Moter, A., Kahl, O., Alberti, G., and Gobel, U.B. 2001. Visualization of *Borrelia burgdorferi* sensu lato by fluorescence in situ hybridization (FISH) on whole-body sections of *Ixodes ricinus* ticks and gerbil skin biopsies. *Microbiology.* **147**:1425–1436.

37. Pal, U., et al. 2004. TROSPA, an *Ixodes scapularis* receptor for *Borrelia burgdorferi*. *Cell* **119**:457–468.

38. Burgdorfer, W., Hayes, S.F., and Corwin, D. 1989. Pathophysiology of the Lyme disease spirochete, *Borrelia burgdorferi*, in Ixodid ticks. *Rev. Infect. Dis.* **11**(Suppl. 6):S1442–S1450.

39. Benach, J.L., Coleman, J.L., Skinner, R.A., and Bosler, E.M. 1987. Adult *Ixodes dammini* on rabbits: a hypothesis for the development and transmission of *Borrelia burgdorferi*. *J. Infect. Dis.* **155**:1300–1306.

40. Zung, J.L., Lewengrug, S., Mrdzibnska, M.A., and Spielman, A. 1989. Fine structural evidence for the penetration of the Lyme disease spirochete *Borrelia burgdorferi* through the gut and salivary tissues of *Ixodes dammini*. *Can. J. Zool.* **67**:1737–1748.

41. Vida, T.A., and Emr, S.D. 1995. A new vital stain for visualizing vacuolar membrane dynamics and endocytosis in yeast. *J. Cell Biol.* **128**:779–792.

42. Kawakami, K., Tatsumi, H., and Sokabe, M. 2001. Dynamics of integrin clustering at focal contacts of endothelial cells studied by multimode imaging microscopy. *J. Cell Sci.* **114**:3125–3135.

43. Balashov, Y.S. 1972. Blood-sucking ticks (Ixodidae)-vectors of disease of man and animals. *Misc. Pub. Entomol. Soc. Am.* **8**:161–376.

44. Schwan, T.G., and Piesman, J. 2000. Temporal changes in outer surface proteins A and C of the Lyme disease-associated spirochete, *Borrelia burgdorferi*, during the chain of infection in ticks and mice. *J. Clin. Microbiol.* **38**:382–388.

45. Sonenshine, D.E. 1993. The midgut. In *Biology of ticks*. D.E. Sonenshine, editor. Oxford University Press. 159–188.

46. Raikhel, A.S. 1983. The Intestine. In *Atlas of ixodid tick ultrastructure*. Y.S. Balashov, editor. Entomological Society of America. College Park, Maryland, USA. 59–97.

47. Charon, N.W., Greenberg, E.P., Koopman, M.B., and Limberger, R.J. 1992. Spirochete chemotaxis, motility, and the structure of the spirochetal periplasmic flagella. *Res. Microbiol.* **143**:597–603.

48. Goldstein, S.F., Charon, N.W., and Kreiling, J.A. 1994. *Borrelia burgdorferi* swims with a planar waveform similar to that of eukaryotic flagella. *Proc. Natl. Acad. Sci. U. S. A.* **91**:3433–3437.

49. Burgdorfer, W., et al. 1982. Lyme disease—a tick-borne spirochetosis? *Science*. **216**:1317–1319.

50. Revel, A.T., Talaat, A.M., and Norgard, M.V. 2002. DNA microarray analysis of differential gene expression in *Borrelia burgdorferi*, the Lyme disease spirochete. *Proc. Natl. Acad. Sci. U. S. A.* **99**:1562–1567.

51. Caimano, M.J., et al. 2007. Analysis of the RpoS regulon in *Borrelia burgdorferi* in response to mammalian host signals provides insight into RpoS function during the enzootic cycle. *Mol. Microbiol.* **65**:1193–1217.

52. Narasimhan, S., et al. 2002. Examination of the *Borrelia burgdorferi* transcriptome in *Ixodes scapularis* during feeding. *J. Bacteriol.* **184**:3122–3125.

53. Ojaimi, C., et al. 2003. Profiling of temperature-induced changes in *Borrelia burgdorferi* gene expression by using whole genome arrays. *Infect. Immun.* **71**:1689–1705.

54. Tokarz, R., Anderton, J.M., Katona, L.I., and Benach, J.L. 2004. Combined effects of blood and temperature shift on *Borrelia burgdorferi* gene expression as determined by whole genome DNA array. *Infect. Immun.* **72**:5419–5432.

55. Cabello, F.C., Godfrey, H.P., and Newman, S.A. 2007. Hidden in plain sight: *Borrelia burgdorferi* and the extracellular matrix. *Trends Microbiol.* **15**:350–354.

56. Hodzic, E., Feng, S., Holden, K., Freet, K.J., and Barthold, S.W. 2008. Persistence of *Borrelia burgdorferi* following antibiotic treatment in mice. *Antimicrob. Agents Chemother.* **52**:1728–1736.

57. Kimsey, R.B., and Spielman, A. 1990. Motility of Lyme disease spirochetes in fluids as viscous as the extracellular matrix. *J. Infect. Dis.* **162**:1205–1208.

58. Charon, N.W., and Goldstein, S.F. 2002. Genetics of motility and chemotaxis of a fascinating group of bacteria: The Spirochetes. *Annu. Rev. Genet.* **36**:47–73.

59. Sauer, J.R., McSwain, J.L., Bowman, A.S., and Essenberg, R.C. 1995. Tick salivary gland physiology. *Annu. Rev. Entomol.* **40**:245–267.

60. Sonenshine, D.E. 1993. Salivary glands. In *Biology of ticks*. D.E. Sonenshine, editor. Oxford University Press. New York, New York, USA. 141–158.

61. Coleman, J.L., and Benach, J.L. 1989. Identification and characterization of an endoflagellar antigen of *Borrelia burgdorferi*. *J. Clin. Invest.* **84**:322–330.

62. Szczepanski, A., Furie, M.B., Benach, J.L., Lane, B.P., and Fleit, H.B. 1990. Interaction between *Borrelia burgdorferi* and endothelium *in vitro*. *J. Clin. Invest.* **85**:1637–1647.

63. Moriarty, T.J., et al. 2008. Real-time high resolution 3D imaging of the Lyme disease spirochete adhering to and escaping from the vasculature of a living host. *PLoS Pathog.* **4**:e1000090.

64. Norman, M.U., et al. 2008. Molecular mechanisms involved in vascular interactions of the Lyme disease pathogen in a living host. *PLoS Pathog.* **4**:e1000169.

65. Eisemann, C.H., and Binnington, K.C. 1994. The peritrophic membrane: its formation, structure, chemical composition and permeability in relation to vaccination against ectoparasitic arthropods. *Int. J. Parasitol.* **24**:15–26.

66. Zhu, Z., Gern, L., and Aeschlimann, A. 1991. The peritrophic membrane of *Ixodes ricinus*. *Parasitol. Res.* **77**:635–641.

67. Yang, X.F., Pal, U., Alani, S.M., Fikrig, E., and Norgard, M.V. 2004. Essential role for OspA/B in the life cycle of the Lyme disease spirochete. *J. Exp. Med.* **199**:641–648.

68. de Silva, A.M., Tyson, K.R., and Pal, U. 2009. Molecular characterization of the tick-*Borrelia* interface. *Front. Biosci.* **14**:3051–3063.

69. Shi, W., Yang, Z., Geng, Y., Wolinsky, L.E., and Lovett, M.A. 1998. Chemotaxis in *Borrelia burgdorferi*. *J. Bacteriol.* **180**:231–235.

70. Hengge, R. 2009. Principles of c-di-GMP signalling in bacteria. *Nat. Rev. Microbiol.* **7**:263–273.

71. Karatan, E., and Watnick, P. 2009. Signals, regulatory networks, and materials that build and break bacterial biofilms. *Microbiol. Mol. Biol. Rev.* **73**:310–347.

72. Wolgemuth, C.W., Charon, N.W., Goldstein, S.F., and Goldstein, R.E. 2006. The flagellar cytoskeleton of the spirochetes. *J. Mol. Microbiol. Biotechnol.* **11**:221–227.

73. Kurtti, T.J., et al. 1993. Adhesion to and invasion of cultured tick (Acarina: Ixodidae) cells by *Borrelia burgdorferi* (Spirochaetales: Spirochaetales) and maintenance of infectivity. *J. Med. Entomol.* **30**:586–596.

74. Comstock, L.E., and Thomas, D.D. 1989. Penetration of endothelial cell monolayers by *Borrelia burgdorferi*. *Infect. Immun.* **57**:1626–1628.

75. Lima, C.M., et al. 2005. Differential infectivity of the Lyme disease spirochete *Borrelia burgdorferi* derived from *Ixodes scapularis* salivary glands and midgut. *J. Med. Entomol.* **42**:506–510.

76. Johns, R., et al. 2001. Contrasts in tick innate immune responses to *Borrelia burgdorferi* challenge: immunotolerance in *Ixodes scapularis* versus immunocompetence in *Dermacentor variabilis* (Acari: Ixodidae). *J. Med. Entomol.* **38**:99–107.

77. Ghosh, A.K., and Jacobs-Lorena, M. 2009. *Plasmodium* sporozoite invasion of the mosquito salivary gland. *Curr. Opin. Microbiol.* **12**:394–400.

78. Ueti, M.W., et al. 2009. Quantitative differences in salivary pathogen load during tick transmission underlie strain-specific variation in transmission efficiency of *Anaplasma marginale*. *Infect. Immun.* **77**:70–75.

79. Frischknecht, F., et al. 2004. Imaging movement of malaria parasites during transmission by Anophelis mosquitoes. *Cell. Microbiol.* **6**:687–694.

80. Sauer, J.R., Essenberg, R.C., and Bowman, A. S. 2000.



- Salivary glands in Ixodid ticks: control and mechanism of secretion. *J. Insect Physiol* **46**:1069–1078.
81. Hubner, A., et al. 2001. Expression of *Borrelia burgdorferi* OspC and DbpA is controlled by a RpoN-RpoS regulatory pathway. *Proc. Natl. Acad. Sci. U. S. A.* **98**:12724–12729.
82. Boardman, B.K., et al. 2008. Essential role of the response regulator Rrp2 in the infectious cycle of *Borrelia burgdorferi*. *Infect. Immun.* **76**:3844–3853.
83. Yang, X.F., Alani, S.M., and Norgard, M.V. 2003. The response regulator Rrp2 is essential for the expression of major membrane lipoproteins in *Borrelia burgdorferi*. *Proc. Natl. Acad. Sci. U. S. A.* **100**:11001–11006.
84. Fraser, C.M., et al. 1997. Genomic sequence of a Lyme disease spirochaete, *Borrelia burgdorferi*. *Nature*. **390**:580–586.
85. Wang, X.G., et al. 2004. Analysis of differences in the functional properties of the substrate binding proteins of the *Borrelia burgdorferi* oligopeptide permease (*opp*) operon. *J. Bacteriol.* **186**:51–60.
86. Fingerle, V., Liegl, G., Munderloh, U., and Wilske, B. 1998. Expression of outer surface proteins A and C of *Borrelia burgdorferi* in *Ixodes ricinus* ticks removed from humans. *Med. Microbiol. Immunol. (Berl.)*. **187**:121–126.
87. Barbour, A.G. 1984. Isolation and cultivation of Lyme disease spirochetes. *Yale J. Biol. Med.* **57**:521–525.
88. Eggers, C.H., et al. 2002. Identification of loci critical for replication and compatibility of a *Borrelia burgdorferi* cp32 plasmid and use of a cp32-based shuttle vector for the expression of fluorescent reporters in the Lyme disease spirochaete. *Mol. Microbiol.* **43**:281–295.
89. Akins, D.R., Bourell, K. W., Caimano, M.J., Norgard, M.V., and Radolf, J.D. 1998. A new animal model for studying Lyme disease spirochetes in a mammalian host-adapted state. *J. Clin. Invest* **101**:2240–2250.
90. Elias, A.F., et al. 2003. New antibiotic resistance cassettes suitable for genetic studies in *Borrelia burgdorferi*. *J. Mol. Microbiol. Biotechnol.* **6**:29–40.
91. Samuels, D.S. 1995. Electrotransformation of the spirochete *Borrelia burgdorferi*. Electrotransformation protocols for microorganisms. *Methods Mol. Biol.* **47**:253–259.
92. Eggers, C.H., Caimano, M. J., and Radolf, J. D. 2004. Analysis of promoter elements involved in the transcriptional initiation of RpoS-dependent *Borrelia burgdorferi* genes. *J. Bacteriol.* **186**:7390–7402.
93. Layne, S.P., Spouge, J.L., and Dembo, M. 1989. Quantifying the infectivity of human immunodeficiency virus. *Proc. Natl. Acad. Sci. U. S. A.* **86**:4644–4648.
94. Spouge, J.L., Layne, S. P., and Dembo, M. 1989. Analytic results for quantifying HIV infectivity. *Bull. Math. Biol.* **51**:715–730.
95. Rasband, W.S. 2009. ImageJ: image processing and analysis in Java. NIH. <http://rsb.info.nih.gov/ij/>.
96. Luna, L.G. 1968. *Manual of histologic staining methods of the Armed Forces Institute of Pathology*. McGraw-Hill. New York, New York, USA. 238–240.
97. Jiang, X., et al. 2005. Histological analysis of GFP expression in murine bone. *J. Histochem. Cytochem.* **53**:593–602.
98. Burgdorfer, W. 1970. Hemolymph test. A technique for detection of rickettsiae in ticks. *Am. J. Trop. Med. Hyg.* **19**:1010–1014.